www.MaterialsViews.com

ADVANCED
OPTICAL
MATERIALS
www.advopticalmat.de

FULL PAPER

# Bioinspired Fabrication of High-Quality 3D Artificial Compound Eyes by Voxel-Modulation Femtosecond Laser Writing for Distortion-Free Wide-Field-of-View Imaging

*Dong Wu, Jian-Nan Wang, Li-Gang Niu, Xu Lin Zhang, Si Zhu Wu, Qi-Dai Chen,\* Luke P. Lee,\* and Hong Bo Sun\**

The small field-of-view (FOV) limits the range of vision in various detecting/imaging devices from biological microscopes to commercial cameras and military radar. To date, imaging with FOV over 90° has been realized with fish-eye lenses, catadioptric lens, and rotating cameras. However, these devices suffer from inherent imaging distortion and require multiple bulky elements. Inspired by compound eyes found in nature, here a small-size (84 μm), distortion-free, wide-FOV imaging system is presented via an advanced 3D artificial eye architecture. The 3D artificial eye structure is accomplished by exploiting an effective optical strategy — high-speed voxel-modulation laser scanning (HVLS). The eye features a hexagonal shape, high fill factor (FF) (100%), large numerical aperture (NA) (0.4), ultralow surface roughness (2.5 nm) and aspherical profile, which provides high uniformity optics (error < ±6%) and constant resolution (FWHM = 1.7 ± 0.1 μm) in all directions. Quantitative measurement shows the eye reduces imaging distortion by two/three times under 30°/45° incidence, compared with a single lens. The distortion-free FOV can be controlled from 30° to 90°.

## 1. Introduction

The most attractive and useful optical functions in nature arise from unique 3D architectures, such as the tapered nanopillar arrays in moth eyes with anti-reflection ability,[1] the periodic micro/nanostructures in butterfly wings with bright color characteristics,[2] and the hundreds of close-packed micro-ommatidium arrays on spherical macro-bases in compound eyes with a distortion-free wide field-of-view (FOV).[3] Scientists have been able to mimic some of those natural structures and realize excellent functions for various applications.[4,5] Among these, 3D biologically inspired compound (BIC) eyes have been highly pursued for wide-angle applications in imaging devices[6–10] and integrated optical microsystems.[11] Compared with other wide FOV devices,[7,12,13] the BIC eyes showed the advantages of small size and distortion-free image.

Natural compound eyes consist of a complex sensing system (Inner: crystalline cone and photoreceptor cells) and imaging system (Outer: hundreds to thousands of ommatidia with a hexagonal shape, 100% fill factor, and a homogenous size of ca. 10–30 μm), which are optimized by thousands of years' selection. For sensing systems (Inner), a lot of artificial devices, such as silicon photodiodes/blocking diodes,[14] self-written waveguides[3] and neuromorphic photodetector[15] have been developed to mimic the crystalline cone and photoreceptor cells (inner) of natural compound eyes. Some of artificial compound eyes exhibited wide FOV, which are great progress towards the application of large-size artificial compound eyes. However, for imaging system (Outer), the lens shape (round), fill factor (ca. 50–70%), and size (ca. 400–1000 μm) of these artificial eyes are much different from those natural ones, which seriously affect resolution and signal-to-noise (Supporting Information, Figure S1).

To pursue high-performance optics of compound eyes, a high fidelity biomimetic imaging system (Outer) is highly desirable and its importance also has been confirmed from Nature. As we know, although there are a variety of compound eyes such as dragonfly, mosquito, fly, butterfly, bees, mantises, ants, spiders, and cicadas, all these compound eyes are hexagonal and 100% fill factor ommatidium with homogeneous size at the magnitude of ca. 10–30 μm. These features are beneficial for high performance optics, e.g., high signal-to-noise and high resolution: i) the ommatidia are optimized as hexagon to realize 100% fill factor so that they ultimately receive the incident light for high signal-to-noise (Supporting Information,

Dr. D. Wu, J.-N. Wang, Dr. L.-G. Niu, X. L. Zhang,
S. Z. Wu, Prof. Q.-D. Chen, Prof. H. B. Sun
State Key Laboratory on Integrated Optoelectronics
College of Electronic Science and Engineering
Jilin University
2699 Qianjin Street, Changchun 130012, China
E-mail: chenqd@jlu.edu.cn; hbsun@jlu.edu.cn
Prof. L. P. Lee
Department of Bioengineering
Department of Electrical Engineering and Computer Science
University of California-Berkeley
Berkeley, CA 94720, USA
E-mail: lplee@berkeley.edu
Prof. H. B. Sun
College of Physics
Jilin University
119 Jiefang Road, Changchun 130023, China

Figure S1): ii) to realize higher resolution imaging, more pixels by smaller-size ommatidia are needed. For example, for 1 cm$^2$ area, there are $100 \times 100$ ommatidia with 10 μm-size and the corresponding 10000 pixels, while there are only $2 \times 2$ ommatidia with 500 μm-size and the corresponding 4 pixels. So, these special features are key important for surviving in Nature. However, present artificial compound eyes prepared by commercial lens-based methods[16,17] and deformed polydimethylsiloxane (PDMS) membrane[3] suffer from round shape, low FF (30–90%), or uncontrollable profile[18] or macrosize due to the inherent limitations of current fabrication methods, which seriously degrades their optical functions. High quality 3D artificial compound eyes (Outer imaging system) remained extremely challenging.

Multiphoton polymerization[19] is considered to be an effective way to realize various 3D complex microstructures[20–22] by point-to-point scanning; however, it is well-known that long fabrication time (ca. tens of hours) limits the fabrication of large-size devices (100–1000 μm) that contain many voxels. This makes the technique unavailable to realize artificial compound eyes that not only have larger size/volume, from hundreds of micrometers to several millimeters, but also require high surface quality, which is crucial for high-precision optical devices. Here we report a distortion-free wide FOV imaging system via advanced BIC eyes, which were realized by exploiting a compromise strategy — high-speed voxel-modulation laser scanning (HVLS). HVLS significantly decreases the fabrication time to within a reasonable range (<10 h), while the surface smoothness remains high (roughness ca. 2.5 nm), which was realized by small scanning voxels. The direct writing strategy ensures that the shape, FF, size, profile of every ommatidium, and the curvature of spherical macrobase can be precisely controlled by optimal program design and threshold laser power. The optical focusing, imaging, and wide FOV of the BIC eye were quantitatively investigated using optical microscopy, intensity scanning, and an oil-assisted optical characterization system.

## 2. Results and Discussion

### 2.1. Natural Compound Eye and High-Quality BIC Eye Prepared by the High-Speed Voxel-Modulation Laser Scanning Method

A biological compound eye[23] consists of an array of thousands of ommatidia arranged on a curved surface (**Figure** 1A) and each ommatidium receives light signals from corresponding directions. Normal incident is mainly transmitted from a crystalline cone behind the ommatidium to the photoreceptor cells. In this way, a wide FOV and distortion-free imaging capability is realized, as shown in Figure 1G and 1H. However, a single lens suffers from strong distortion under tilted incident light, according to theoretical simulation (Figure 1E and 1F). The magnified scanning electron microscopy (SEM) image in Figure 1B shows that the ommatidia are homogeneous, ca. 16 μm in diameter with a height of ca. 4 μm. Moreover, the hexagonal shape of the ommatidium provides a 100% FF to ultimately utilize the incident light and ensure a high signal-to-noise ratio (SNR), which is evidenced by theoretical simulation of the

focusing properties of BIC eye with and without gaps between the ommatidium (Supporting Information, Figure S1). The SNR for BIC eye without gaps is 2.23, which is much larger than that with gaps (1.28).

Laser direct writing is a promising method to realize such complex 3D morphology; however, there is much difficulty in fabricating large-volume microstructures with high precision due to unreasonable fabrication times. For example, the theoretical time for the fabrication of a 320 μm sized eye by conventional precise scanning (voxel distance = 100 nm × 100 nm × 100 nm) is as much as 870 h (Supporting Information, Figure S2C). On the other hand, although large voxel (ca. 500 nm × 500 nm × 500 nm) scanning could reduce the time to less than 6.96 h (Supporting Information, Figure S2C), this would lead to high surface roughness. Here, a novel scanning concept is proposed (Figure 1I), where the outer part of the microstructures (ommatidia) is precisely defined by a small voxel while the inner part (spherical base) is rapidly scanned by a large voxel. This will make it possible to fabricate BIC eye with both high quality and within a reasonable time. Figure 1C and 1D show top-view and 30°-tilted SEM images of 84 μm-size artificial compound eye fabricated by the HVLS method (400 nm × 400 nm × 100 nm) in a commercial epoxy-based negative resin SU-8[24,25] as a proof-of-concept. The size and the number of ommatidia (ca. 150) is approximate to natural ant compound eyes (Supporting Information, Figure S2E and S2F). 3D laser confocal images (Supporting Information, Figure S4B and S4D) and a 90°-tilted SEM image (Supporting Information, Figure S4C) indicate a profile height of 20 μm, which corresponds well with the designed model. The BIC eye costs only 0.85 h for $3.04 \times 10^6$ voxels while the time for precise scanning ($4.86 \times 10^7$ voxels) is as much as 13.6 h. Even for 160 μm-size eyes, the time for HVLS (400 nm × 400 nm × 400 nm) is only 1.7 h. However, the time for conventional mode (100 nm × 100 nm × 100 nm) is 108.8 h (Supporting Information, Figure S2C) and is unavailable. The time for HVLS can be further shortened by bigger voxel (ca. 1 μm),[26] which makes it possible to realize larger size BIC eyes and have the potential to solve the bottleneck of laser direct writing in the fabrication of devices/systems with both large size and high precision. The surface roughness of flat surface by HVLS was as small as 2.5 nm (Supporting Information, Figure S4B). For comparison, ommatidia were prepared by 400 nm-voxel scanning, and there were significant solenoid traces (Supporting Information, Figure S4E) caused by the bigger voxel spacing. This demonstrated that this HVLS strategy not only decreased the fabrication time to a reasonable range, but also maintained ultrahigh surface smoothness. Moreover, these ommatidia were designed by optimized computer program as hexagonal shape and 100% FF, which is highly comparable to natural compound eyes. The NA determined by the ratio of the lens height to the diameter ($h/d$ ca. 2/8, Supporting Information, Figure S4C) was approximately 0.4, which is similar to the NA for a natural eye ($h/d$ ca. 4/16). The profile was optimized as an aspherical lens with reduced spherical aberration, as reported in a previous demonstration of 20 nm precision by optimal threshold laser power (ca. 6 mW, Supporting Information, Figure S3) on a flat surface.[27] All these optimal parameters ensured high optical performance of the BIC eye.
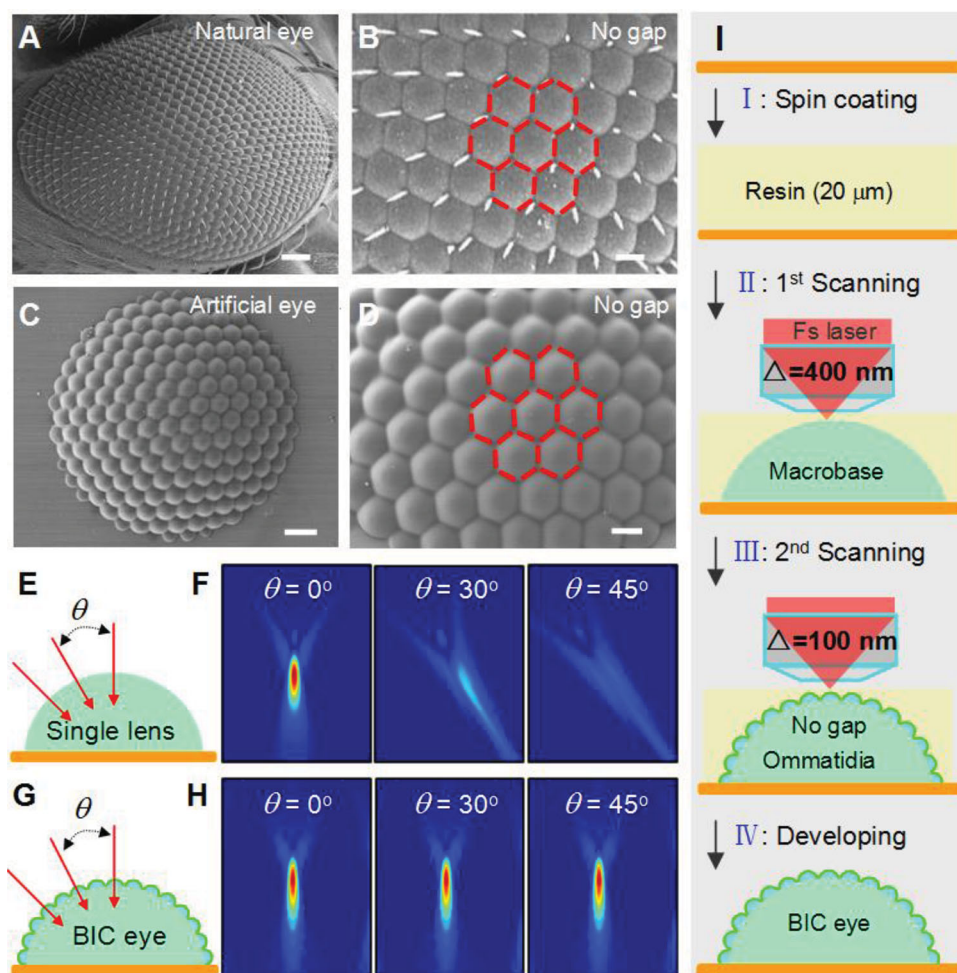
Materials Views
www.MaterialsViews.com

ADVANCED
OPTICAL
MATERIALS
www.advopticalmat.de

FULL PAPER

**Figure 1.** Natural compound eye and high quality BIC eye prepared by the high-speed voxel-modulation laser scanning method. A,B) Top-view and magnified SEM images of a natural compound eye showing macrobase and hundreds of hexagonal 100% fill-factor micro-ommatidia. C,D) Top-view and 30°-tilted magnified SEM images of the BIC eye; the 100% FF of hexagonal ommatidia is comparable to natural one in (B). The scale bars in (A–D) are 40, 10, 10, and 5 µm, respectively. E–H) Comparison of the FDTD theoretical simulated intensity distribution for light incident from various angles (0 to 45°) onto a single microlens and BIC eye. I) Schematics for the fabrication of BIC eye by the HVLS method, which enables reasonable fabrication times while maintaining high quality. The inner macrobase is scanned by large voxels ($\Delta$ = 400 nm) while the outer surface is fabricated by small voxels ($\Delta$ = 100 nm).

## 2.2. Characterizations of Imaging and Optical Uniformity of Artificial Compound Eye

To character the optical property of BCE, a system comprising a halogen lamp, a 3D positioning stage, a 60× objective lens and a charge coupled device camera was set up (Supporting Information, Movie S1). The BIC eyes exhibit high optical uniformity and imaging functions. As shown in **Figure 2**A–C and in Movie S1 in the Supporting Information, imaging was clearly observed when the letters "P", "L" and "T" were placed in front of the BIC eyes. Another notable feature of the BIC eyes is the high optical uniformity of the ommatidia along the 360° direction of the XY plane. When light was incident onto the BIC eyes, every ommatidium produced a focal spot. The focal spot from the central part of the BIC eye (Figure 2D) was firstly detected when the OL was moved from near to far. The focal spots from the middle (Figure 2E) and outer parts (Figure 2F, and Movie S2 in the Supporting Information) were then observed. To

quantify the optical focusing, the grayscale intensities of the focal spots were extracted from six symmetrical positions, as shown in Figure 2G–I. The errors were less than ±6%. The peak intensity (189 ± 2 in Figure 2G) of the focal spot at the central part of BIC eyes was larger than those (171 ± 4 in Figure 2H and 79 ± 5 in Figure 2I) at the middle and outer parts of the BIC eye because the incident light was not perpendicular to those ommatidia.

## 2.3. Computational and Experimental Measurement of Wide FOV Imaging with a BIC Eye and Single Lens

The most important parameter for the BIC eye was the FOV. Besides fabrication difficulties of imaging system, there is also a lack of effective optical sensing systems with which to characterize FOV. Silicon diodes and neuromorphic photodetector have been developed for ommaditium with bigger size
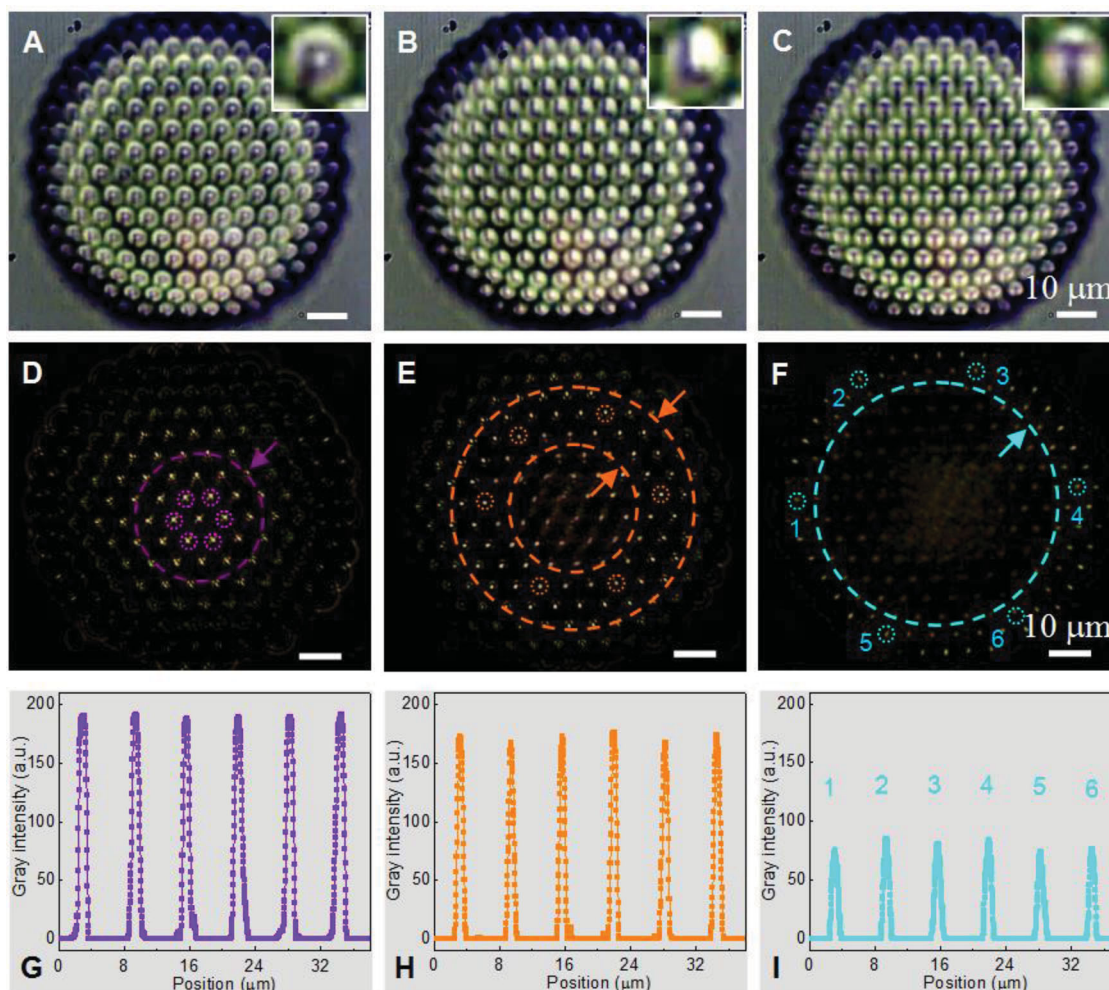
**Figure 2.** Characterizations of imaging and uniformity of compound eye. A–C) Imaging of the letters "P", "T", and "L" by the central ommatidia. Those ommatidia at the side of the BIC eye do not exhibit good imaging ability, which was not caused by the quality of the BIC eye, but by the large spherical base, because the incident light was not perpendicular to those ommatidia. D–F) Different focal spots from the central, middle, and outer side parts of the BIC eye when the OL was moved from near to far. G–I) Grayscale intensities of the focal spots from six symmetrical positions that demonstrate high uniformity (error < ±6%).

(ca. 400–1000 μm). Here, for our BIC eyes with such a smaller size (ca. 8 μm) ommatidium, an in-house built oil-assisted rotating-lens method was developed (**Figure 3**A). The oil (Figure 3B–D) was used to eliminate the total reflection and refraction at the interface between the air (n = 1) and glass substrate (n = 1.515 for 632 nm wavelength) (Supporting Information, Figure S5A and S5B) because the refractive index of the oil (ca. 1.52) was approximately the same as that of the glass and the BIC eye (ca. 1.58). The incident light was first collected by the ommatidium, transmitted through the oil, magnified by an objective lens (OL) and detected with a CCD. The incident angle was changed using reflective mirror 1 (M1 in Figure 3A). When light was incident from a certain angle, e.g. 30°, the OL was rotated to better receive the light signal (Supporting Information, Figure S5C). Similarly, in natural compound eyes, many interior photoreceptors on a curved surface are used to detect light signals from different directions.[3,28] It is also noteworthy that an OL with a long

work-distance (ca. 4 mm, 60×) is crucial to achieve sufficient distance between the OL and BIC eye during rotation of the OL, while a conventional high NA oil-immersion OL with a short work-distance (ca. 200 μm) is not suitable. Figure 3J–L show the θ = 0, 30°, and 45° light signals received by the BIC eye (Figure 3I). The focal spots kept round and sharp, which was consistent with the theoretical simulation (Figure 3J–L insets). This demonstrates that the BIC eye achieved a wide FOV of 2θ that was larger than 90° and approximately the same as the theoretical value of 97°. Even the incident angle is bigger than 50°, the BIC eye can still receive the incident light. In this case, a slight distortion happened (Supporting Information, Figure S6). However, a single lens (Figure 3E) exhibited significant imaging distortion when the light was incident from tilted angles of 30° and 45° (Figure 3G,H), which was consistent with the theoretical intensity distribution simulated by the finite difference time domain (FDTD) method (Figure 3G,H insets).
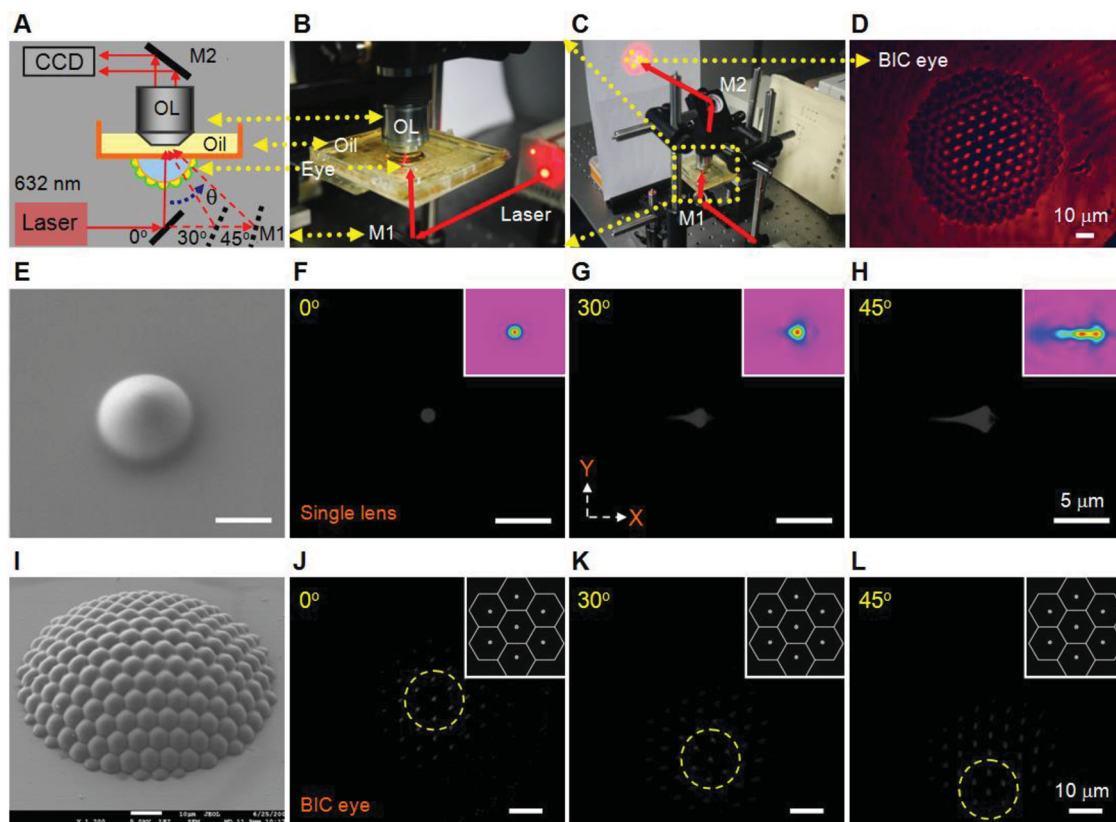
**Figure 3.** Computational and experimental results of wide FOV imaging with a BIC eye and single lens, and the oil-assisted optical characterization system. A–D) Schematic image (A) and digital photos (B,C) of the overall optical characterization system and the BIC eye (D). The oil-assisted method allows the original refraction and total reflection effect on the interface between the BIC eye and the air to be eliminated. E–H) 45°-tilted SEM image of a single microlens and the corresponding focus properties. The focal spots exhibit significant imaging distortion under tilted incident light, while no deformation was observed with the BIC eye. I–L) 45°-tilted SEM image of the BIC eye and the light collected by the BIC eye under various incident angles (0, 30, and 45°). The insets in F–H and J–L show the theoretical normalized intensity distributions.

## 2.4. Quantitative Characterization and Comparison of the FOV Properties of Single Lens / Artificial Compound Eye

To quantify the optical performance of the BIC eye, the point spread functions (PSF) along both x and y-axes were measured (Figure 4C and 4D) from optical microscope images. The full width at half maximum [FWHM, 1.7 ± 0.1 μm (x-axis) and 1.9 ± 0.2 μm (y-axis) at 632 nm measured at the half intensity between the biggest (ca. 1) and the average noise intensity (ca. 0.1–0.2)] remained constant, even under tilted incident light, which indicates the wide FOV capability of BIC eye without imaging distortion. The small difference in the focal sizes along the x and y-axes may be caused by that the incident light during the experiment, which did not have absolutely normal incidence. However, for a single lens, the FWHM (x/y-axis) increased from 1.6 ± 0.1/1.7 ± 0.1 μm to 3.4 ± 0.1/2.4 ± 0.2 μm and 5.4 ± 0.2/3.2 ± 0.1 μm when the incident angle was changed from 0° to 30 and 45° (Figure 3A and 3B), respectively. The BIC eye had reduced imaging distortion by 2 and 3 times along the x-axis, and by 1.3 and 1.7 times along the y-axis under 30 and 45° incident light compared with that for the single lens.

## 2.5. Angular-Sensitivity Function and Controllable FOV by Adjusting the Base Height of the BIC Eye

Furthermore, the angular sensitivity function (ASF) (**Figure 5**A and Table S1 in the Supporting Information) was characterized by measuring the relative intensity of the light at the distal end of each ommatidium, which followed a Gauss distribution by theoretical fitting. It was found that the intensity received by the ommatidium decreased to 0.5 when the light is incident at the title angle of ca. 15.2°, which was wider than the interommatidial angle (ca. 7.4°, Supporting Information, Figure S7) of the BIC eye. This will lead to the optical crosstalk between two adjacent ommatidia due to the fabrication difficulty of the limiting optical components in such a smaller-size BIC eye. But, the cross-talk was significantly decreased between the non-adjacent ommatidia (e.g., the 2nd and 4th ommatidia, the 5th and 7th ommatidia, in Figure 5A and Table S1 in the Supporting Information) because the focusing ability of the ommatidia became weak under the tilted light incident. In addition, the optical crosstalk could be further reduced by introducing self-written waveguides (3) to avoid overlap-induced imaging degradation.
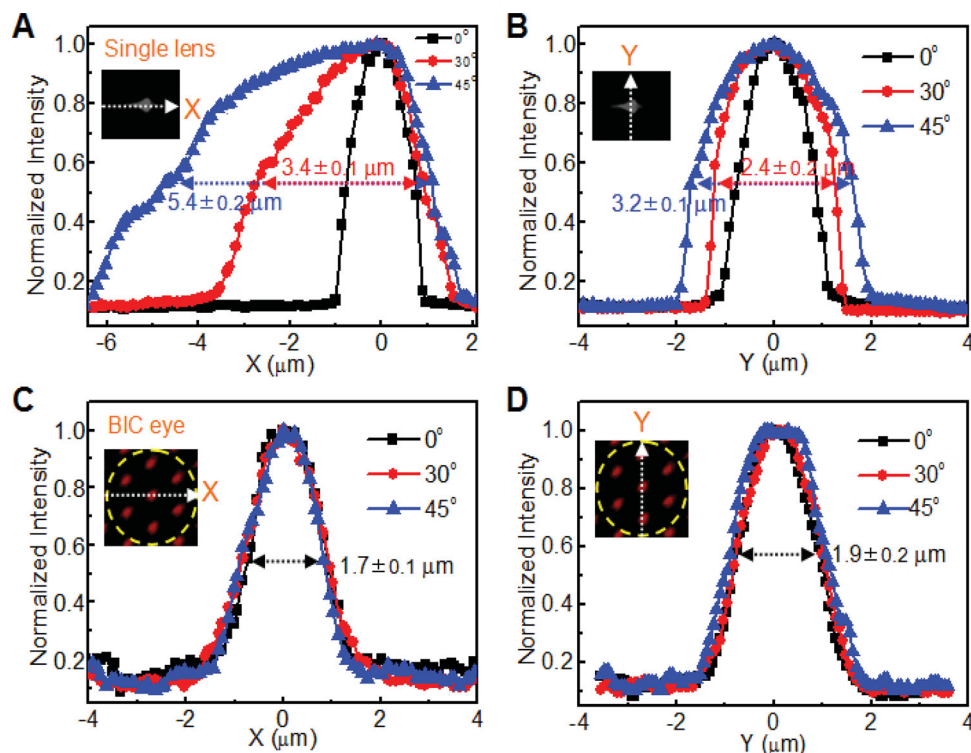
**Figure 4.** Quantitative characterization of the FOV properties of single lens / compound eye. A,C) Comparison of x-direction PSF for the single micro-lens and BIC eye; the imaging distortion of the BIC eye was reduced by 2 and 3 times under 30 and 45° light incidence compared with that for the single microlens. The insets in (A) and (C) are the focus spots of the BIC eye under 30° light incidence. B,D) Y-direction PSF of the BIC eye and single microlens. The BIC eye had reduced imaging distortion by 1.3 and 1.7 times along the y-axis under 30 and 45° incident light compared with that for the single lens.

The ability to control the FOV and realize different BIC eyes will be needed for various potential applications. According to numerical deduction, the theoretical FOV is given by:

$$FOV = 2 \times \arcsin\left( 2Rh / R^2 + h^2 \right)$$

The FOV was determined from the height (h) and radius (R) of the spherical base, as shown by the curve in Figure 5B. Thus, the FOV could be precisely tuned for various practical applications by controlling h and R. BIC eyes were designed with different FOVs by adjusting h, while R was kept constant. From the theoretical curve of FOV vs. h, h was deduced to be 5.3, 10.7, and 16.5 μm for 30, 60, and 90°, respectively, and the curvature radii were 154, 80, and 57 μm. The corresponding BIC eyes were realized by the HVLS approach and are shown in the insets of Figure 5B.

## 3. Conclusion

This work demonstrates the biomimetic fabrication of high quality BIC eyes by exploiting a VLMS strategy. The improved direct writing strategy can realize BIC eyes that feature a high FF (100%), large NA (0.4), ultralow surface roughness (2.5 nm), and an aspherical profile. The oil-assisted optical characterization system showed that the BIC eye significantly reduces imaging distortion by 2 times and 3 times under 30° and 45° light incidence, compared with that for a single lens. Furthermore, the

BIC eye demonstrated imaging and high uniformity optics (<±6%) in all directions. By controlling the heights of the spherical macrobase at 5.3, 10.7 and 16.5 μm, distortion-free wide FOV imaging of 30, 60, and 90° was demonstrated.

Besides single BIC eyes, the HVLS strategy could be used to fabricate a pair of BIC eyes similar to those observed in nature which exhibit FOV greater than 180°. More importantly, this method has afforded considerable potential for the preparation and integration of various large-volume 3D optical elements and functional micromachines with electronic components, silicon photonics[7,8] and microfluidic devices,[29] and will be beneficial to CMOS and optofluidic technologies.[14] Besides the fabrication of high fidelity BIC eyes along natural ones, their CMOS integration is also an important direction towards practical application. For example, Song et al. combined elastomeric microlenses with silicon photodiodes to realize wide FOV digital cameras (size ≈ 1.4 cm).[15] So, with the further development of microfabrication in future, the smaller-size high-performance BIC eyes could also be combined with photoelectrical microreceivers or optical devices for a broad range of applications, such as wide-angle communication antenna,[4] integrated optical circuits, and so on.

## Experimental Section

*Sample Preparation*: Photoresist samples were prepared by spin-coating SU-8 (NANO, MicroChem) films on microscope cover slides.
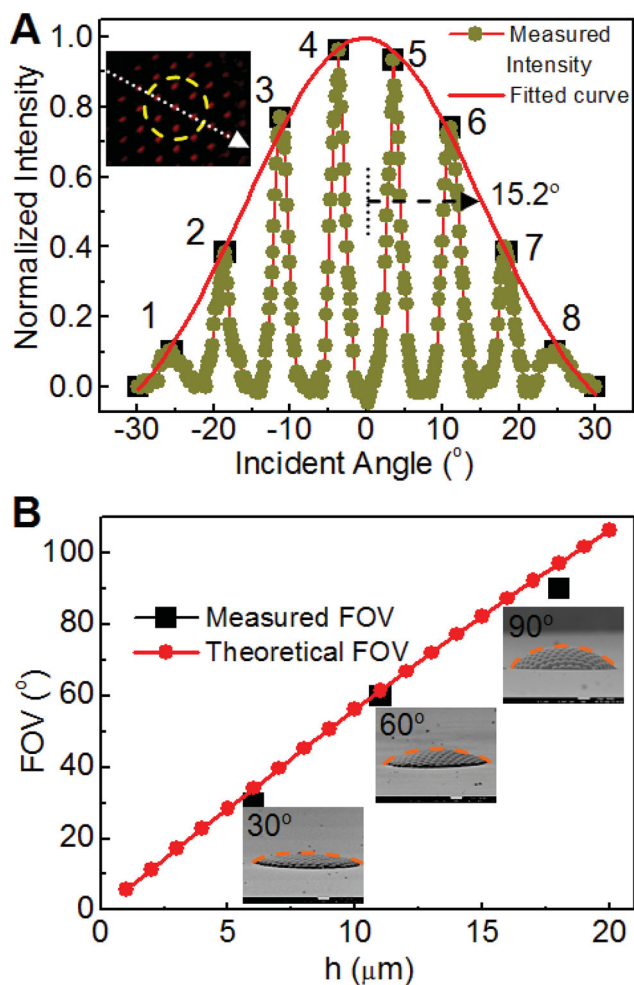
**Figure 5.** Angular sensitivity function and controllable FOV by adjusting the base height. A) ASF of the BIC eye measured from the scanning profiles of color intensities from optical microscopy images (inset). The intensity received by the ommatidium decreased to 0.5 when the light is incident at the title angle of ca. 15.2° (> the interommatidial angle of 7.4°) which will lead to the optical crosstalk between two adjacent ommatidia due to the fabrication difficulty of the limiting optical components in such a smaller-size BIC eye. But, the crosstalk was significantly decreased between the non-adjacent ommatidia (e.g., the 1st and 3rd ommatidia, the 2nd and 4th ommatidia) because the focusing ability of the ommatidium became weak under the tilted light incident (Supporting Information, Table S1). B) Tuning the FOV values by adjusting the base height. The curve is the theoretical relationship between the base height (h) and the FOV when the base radius is kept constant at 40 μm. The insets show cross-sectional SEM images of BIC eye with various FOVs of 30°, 60°, and 90° and corresponding heights of the large spherical base are 5.3, 10.7, and 16.5 μm, respectively.

The SU-8 thick films (ca. 25 μm) were then soft baked at 95 °C for 30 min to evaporate the solvent. A femtosecond laser pulses (790 nm peak wavelength, 120 fs pulse width, 80 MHz repetition rate) were focused into the resin with a high numerical aperture (NA = 1.4) 100× oil immersion objective lens (OL). The focal spot was scanned laterally by steering a two-galvano-mirror set and scanned along the optical axis with a piezo stage (Physik Instrument). The large spherical base was first rapid scanned with a large voxel spacing (400 × 400). The laser exposure power was sufficiently high (15 mW) to ensure that the adjacent voxels could connect with each other. The ommatidia were then precisely defined (100 × 100) under a lower laser power (6 mW) around

the SU-8 photopolymerization threshold. The high surface quality of the BIC eyes was further ensured by a feedback system to stabilize the laser pulse energy and the self-smoothing effect.[30] Upon irradiation with the femtosecond laser, the photoinitiator generated an acid by two-photon absorption with a spatial concentration that followed the distribution of the square of light intensity. In a post-exposure bake with a temperature ramp from 65 to 95 °C for 10 min, the latent image was converted to a dense crosslinking by chain reaction. The degree of crosslinking determined the solubility in the developing solvent (GBL). Resin that was sufficiently illuminated remained, whereas the underexposed resin was removed by the solvent. The sample was developed in SU-8 developer for 60 min to remove unsolidified liquid resin. After drying, the fabricated microstructures were obtained.

*FOV Measurement*: A container was set with a 3 mm × 3 mm-width hole at the bottom. The BIC eye sample was placed onto the bottom of the container and in the middle of the hole and was secured with adhesive tape. Oil was then added to the container and a long work-distance OL was immersed into the oil. A 632 nm laser was used as the incident light source. The laser light was first incident onto the BIC eye sample and then transmitted to the oil region where the light signal was magnified by the OL and received by a CCD or projected to a blank screen.

*FDTD Simulation*: The structure considered in this study was a single microlens of which the optical focusing properties were investigated using the finite difference time domain (FDTD) model of the RSoft method. The refractive indices of dielectrics used are $n_{su-8} = 1.58$ and $n_{air} = 1$. The diameter and height of a single microlens were 8 and 2 μm, respectively. The measured focal length is about 10 μm. Plane wave excitation under various incident angles (0, 30, and 45°) onto the single microlens was assumed in the FDTD calculations. The intensity distribution of the structure was obtained, as shown in Figure 1F and 1H, and the insets of Figure 3F–H and 3J–L.

## Supporting Information

Supporting Information is available from the Wiley Online Library or from the author.

## Acknowledgements

[1] C. G. Bernhard, *Endeavour* **1967**, *26*, 79.
[2] A. R. Parker, H. E. Townley, *Nat. Nanotechnol* **2007**, *2*, 347.
[3] K.-H. Jeong, J. Kim, L. P. Lee, *Science* **2006**, *312*, 557.
[4] Y. F. Huang, S. Chattopadhyay, Y. J. Jen, C. Y. Peng, T. A. Liu, Y. K. Hsu, C. L. Pan, H. C. Lo, C. H. Hsu, Y. H. Chang, C. S. Lee, K. H. Chen, L. C. Chen, *Nat. Nanotechnol.* **2007**, *2*, 770.
[5] M. Kolle, P. M. S. Cunha, M. R. J. Scherer, F. Huang, P. Vukusic, S. Mahajan, J. J. Baumberg, U. Steiner, *Nat. Nanotechnol.* **2010**, *5*, 511.
[6] M. G. L. Gustafsson, *Proc. Nat. Acad. Sci. USA* **2005**, *102*, 13081.
[7] B. Micusik, T. Pajdla, *IEEE Trans. Pattern Anal. Mach. Intell.* **2006**, *28*, 1135.
[8] J. Feinberg, *Opt. Lett.* **1983**, *8*, 480.

FULL PAPER

[9] S. Jivkova, M. Kavehrad, *IEEE Trans. Commun.* **2001**, *49*, 2145.

[10] A. E. Spezio, *IEEE Trans. Microwave Theory Tech.* **2002**, *50*, 633.

[11] Q.-F. Xu, B. Schmidt, S. Pradhan, M. Lipson, *Nature* **2005**, *435*, 325.

[12] D. Gledhill, G. Y. Tian, D. Taylor, D. Clarke, *Comput. Graphics* **2003**, *27*, 435.

[13] M. F. Land, D.-E. Nilsson, *Oxford Animal Biology Series*, Oxford University Press, Oxford, UK, **2002**.

[14] Y. M. Song, Y. Xie, V. Malyarchuk, J. Xiao, I. Jung, K. J. Choi, Z. Liu, H. Park, C. Lu, R. H. Kim, R. Li, K. B. Crozier, Y. Huang, J. A. Rogers, *Nature* **2013**, *497*, 95.

[15] D. Floreano, R. P. Camara, S. Viollet, F. Ruffier, A. Bruckner, R. Leitel, W. Buss, M. Menouni, F. Expert, R. Juston, M. K. Dobrzynski, G. L. Eplattenier, F. Recktenwald, H. A. Mallot, N. Franceschini, *Proc. Natl. Acad. Sci. USA* **2013**, *110*, 9267.

[16] F.-H. Zhao, Y.-J. Xie, S.-P. He, S.-J. Fu, Z.-W. Lu, *Opt. Express* **2005**, *13*, 5846.

[17] D. Radtke, J. Duparre, U. D. Zeitner, A. Tunnermann, *Opt. Express* **2007**, *15*, 3067.

[18] H. Liu, F. Chen, Q. Yang, P. Qu, S. He, X. Wang, J. Si, X. Hou, *Appl. Phys. Lett.* **2012**, *100*, 133701.

[19] P. Tayalia, C. R. Mendonca, T. Baldacchini, D. J. Mooney, E. Mazur, *Adv. Mater.* **2008**, *20*, 4494.

[20] B. Kaehr, J. B. Shear, *Proc. Natl. Acad. Sci. USA* **2008**, *105*, 8850.

[21] L.-J. Li, R. R. Gattass, E. Gershgoren, H. Hwang, J. T. Fourkas, *Science* **2009**, *324*, 910.

[22] Y.-L. Sun, W.-F. Dong, L.-G. Niu, T. Jiang, D.-X. Liu, Y.-S. Wang, D.-P. Kim, Q.-D. Chen, H.-B. Sun, *Light Sci. Appl.* **2014**, *3*, e129.

[23] M. Deubel, G. V. Freymann, M. Wegener, S. Pereira, K. Busch, C. M. Soukoulis, *Nat. Mater.* **2004**, *3*, 444.

[24] K. K. Seet, V. Mizeikis, S. Matsuo, S. Juodkazis, H. Misawa, *Adv. Mater.* **2005**, *17*, 541.

[25] W. H. Teh, U. Durig, U. Drechsler, C. G. Smith, H.-J. Guntherodt, *J. Appl. Phys.* **2005**, *97*, 054907.

[26] D. Wu, Q. D. Chen, L. G. Niu, J. Jiao, H. Xia, J. F. Song, H. B. Sun, *IEEE Photonics Technol. Lett.* **2009**, *21*, 1535.

[27] P. V. Braun, *Progress in Sensory Physiology*, (Ed. D. Ottoson), Springer-Verlag, Berlin, Germany, **1985**, pp. 1–79.

[28] D. Wu, Q. D. Chen, L. G. Niu, J. N. Wang, J. Wang, R. Wang, H. Xia, H. B. Sun, *Lab Chip* **2009**, *9*, 2391.

[29] C. Monat, P. Domachuk, B. J. Eggleton, *Nat. Photonics* **2007**, *1*, 106.

[30] K. Takada, H. B. Sun, S. Kawata, *Appl. Phys. Lett.* **2005**, *86*, 071122.